Accepted Manuscript

Ab initio study of the role of defects on the magnetic response and the structural, electronic and hyperfine properties of $ZnFe_2O_4$

J.J. Melo Quintero, K.L. Salcedo Rodríguez, C.E. Rodríguez Torres, L.A. Errico

Please cite this article as: J.J. Melo Quintero, K.L. Salcedo Rodríguez, C.E. Rodríguez Torres, L.A. Errico, Ab initio study of the role of defects on the magnetic response and the structural, electronic and hyperfine properties of $ZnFe_2O_4$, *Journal of Alloys and Compounds* (2018), doi: https://doi.org/10.1016/j.jallcom.2018.10.082.

Ab initio study of the role of defects on the magnetic response and the structural, electronic and hyperfine properties of ZnFe$_2$O$_4$. `

J. J. Melo Quintero[1], K. L. Salcedo Rodríguez[1], C. E. Rodríguez Torres[1], and L. A. Errico[1,2].

[1] Departamento de Física, Facultad de Ciencias Exactas, Universidad Nacional de La Plata (UNLP) and Instituto de Física La Plata, IFLP-CONICET CCT-La Plata, 1900, La Plata, Argentina.

[2] Universidad Nacional del Noroeste de la Provincia de Buenos Aires (UNNOBA), Monteagudo 2772, 2700 Pergamino, Buenos Aires, Argentina.

In this work the effects of defects (oxygen vacancies, cationic inversion) on the structural, electronic and the magnetic response of the spinel ZnFe$_2$O$_4$ (ZFO) are studied by using a density functional theory (DFT) based *ab initio* method (the Full-Potential Linearized Augmented Plane Waves plus Local Orbitals, LAPW+lo) on the framework of the Generalized Gradient Approximation plus U (GGA+U) level. The changes induced by the defects in the hyperfine interactions at the Fe sites of the structure are also presented. In order to discuss the magnetic ordering and the electronic structure of the system we considered different spin arrangements. We found that, similar to the normal and pristine case, reduced and partially inverted ZFO presents an energy landscape characterized by a large number of metastable states. Our calculations successfully describe the hyperfine properties (isomer shift, magnetic hyperfine field and quadrupole spliting) at the Fe sites that are seen by Mössbauer Spectrocopy (MS) at 4 and 300 K, enabling us to characterize the local structure around Fe atoms. Our LAPW+lo predictions also demonstrate the relevance of both oxygen vacancies and antisites (cationic inversion) in the formation of local ferromagnetic coupling between Fe ions, giving rise to a

ferrimagnetic ordering in an otherwise antiferromagnetic compound. This results support conclusions based in experimental results obtained in x-ray magnetic circular dichroism and magnetization measurements performed on zinc ferrites with different cation distributions and oxygen vacancy concentrations reported in the literature.

2. Introduction

Transition-metal oxides exhibit an incredibly wide variety of behaviours. They can be insulators, semiconductors or metals and present properties such as ferroelectricity, magnetism or superconductivity. Different types of defects (vacancies, antisites, structural distortions, surface effects, substitutional or interstitial impurities, among others) play a fundamental role in the origin of these properties and behaviours. Then, understanding the relation defect-properties is fundamental for the development of new functionalities, for example spintronics [1-3]. The main goal in this field is to obtain materials that can be semiconducting and ferromagnetic at room temperature and integrate them into heterostructures that could be used as spin valves and spin filters.

Within the set of oxides that have been considered for their possible application in spintronics, ferrites ($M\text{Fe}_2\text{O}_4$) have emerged as a very interesting possibility [4, 5]. Ferrites crystallize in the spinel face-centered cubic structure and are characterized by an atomic arrangement of two sites for the cations: sites A (tetrahedral oxygen coordination) and sites B (octahedral oxygen coordination) [6]. Two types of ferrites can be distinguished, normal and inverted. In the first case, the M ions occupy the A sites and the Fe ions occupy the B sites. In the case of the inverted ferrites, the A sites are populated by Fe ions and the M and Fe ions occupy the B sites in the same proportion. There are also cases of partial inversion. The magnetic coupling in ferrites is governed by super-exchange between the metal cations via oxygen atoms, resulting in A-O-A, B-O-B and A-O-B couplings [7, 8]. Then, the magnetic properties of ferrites strongly depend on the cation distribution in both sub-lattices [8].

Among the ferrite group, Zn ferrite ($ZnFe_2O_4$, ZFO) is of particular interest not only in basic research but also due to their extensive technological applications [9-16]. ZFO ferrite is used for the fabrication of magnetic materials [14, 17] and has an important role as absorbent in desulphurization process [18] and due to their capability to absorb visible light and its high efficiency, ZFO is a promising photo-catalyst semiconductor for various processes such as photo-induced transformer, photo-electrochemical cells and photochemical hydrogen production [19-22].

In basic research, the underlying magnetism of ZFO has been of interest over the last four decades [23-32] and several studies were performed using a large variety of experimental techniques until now. In cases where *M* is a non-magnetic metal (Zn, for example) and normal ferrites (as in the case of ZFO) the Fe ions occupy solely the *B* sites and only *B*-O-*B* interactions occur. Since the magnetic coupling between the Fe atoms on the *B*-sublattice is weak, ZFO is widely identified as an antiferromagnet with a Néel temperature (T_N) around 10 K. But the situation is not so simple. Neutron diffraction experiments [23, 26] demonstrated that the ground state of ZFO is characterized by a complex antiferromagnetic spin structure and is susceptible to geometrical frustration [24, 25, 27], a fact that can give rise to a variety of fundamental magnetic states such as ferrimagnetism, local spin canting, and glassy magnetic behaviours [29, 33-36]. In this sense, Schiessl *et al*. [23] performed extensive studies (using neutron diffraction and other techniques) on the magnetic properties of ZFO. They found that below 10 K a short and a long range orders coexist. Yamada *et al*. [25] and Usa *et al*. [27] claimed that ZFO remains magnetically disordered even at temperatures as low as 1.5 K and suggest that the long-range magnetic order is driven by quenched atomic disorder, allowing the interpretation of ZFO as an intrinsically frustrated spin system. Field cooled and zero-field cooled DC magnetization experiments [29] suggest that ZFO presents a spin-glass phase at low temperatures and Yamada *et al*. [25] and Tomiyazu *et al*. [37] proposed a molecular spin model for the ground state of ZFO that is consistent with the neutron scattering data [26].

In the previously mentioned studies bulk samples and a normal structure for ZFO was assumed. Indeed, rarely ZFO can be obtained in a pure normal state but somewhat inverted.

Depending on the method and growth conditions of the sample [7, 38, 39, Ref. 5 and references therein], or when the characteristic lengths of the sample are reduced to the nanoscale [32], meta-stable phases can be formed with a disordered arrangement of Zn and Fe in sites *A* and *B*. In consequence, depending on the synthesis method or the dimensions of the sample, changes in the Fe-Fe interactions (and therefore in the magnetic response of the system) can occur. As an example, Pandey *et al*. [32] and Jesus *et al*. [33] showed that thin films or ZFO-nanoparticles present ferromagnetic behaviour at high temperatures. This result was attributed to cationic inversion [40]. Stewart et al. [41] demonstrated by X-Ray Absorption Near Edge Spectroscopy (XANES), magnetic circular dichroism (XMCD) and Mössbauer spectroscopy (EM) that ZFO nanoparticles that present cationic inversion exhibit ferrimagnetism at room temperature and concluded that the cationic inversion (and not necessarily the size-effects) is the factor that modifies the long-range magnetic order and increases the magnetic moment of the system. Similarly, Nakashima *et al*. [39] reported the effects of cationic inversion on the XANES spectra of ZFO films deposited by sputtering. From the comparison of the experimental XANES spectra and those obtained by means of *ab initio* calculations, they inferred the presence of some degree of inversion in their samples. In addition, through successive thermal treatments, observed that the inversion-degree decreased while the magnetic behavior changes from an antiferromagnetic to a spin-glass. This effect was associated to the dominating interaction (*A*-O-*A*, *A*-O-*B*, *A*-O-*A*) for a given inversion-degree.

The oxygen concentration also seems to be crucial for the magnetic response of ZFO since samples grown under low oxygen pressure show a large magnetic response at room temperature [26, 42, 43]. Rodríguez Torres *et al*. [5] studied how the variation of oxygen pressure during the growth process of ZFO films modifies its magnetic response. By means of XMCD experiments and *ab initio* calculations they have proved that the formation of oxygen vacancies can be at the origin of the ferrimagnetic response of ZFO. This result is in agreement with those found for other transition-metal oxides in which ferromagnetic coupling between cations can be associated to the presence of a sufficiently high concentration of oxygen vacancies in a certain region of the material [44, 45].

From the theoretical point of view, realistic theoretical studies of ZFO (besides those previously mentioned) are scarce and in general have been limited to study structural and electronic properties for the case of the pristine and normal structure. We must cite here the *ab initio* study performed by Ching Cheng [46], in which the author predicts that normal ZFO presents topological frustration and that the system will remain in a paramagnetic state still at 0 K. More recently, some of us presented an *ab initio* study of the structural, electronic and magnetic properties of pristine ZFO [47].The calculations revealed that the energy landscape of ZFO is characterized by a large number of closed local energy minima, pointing to a spin-glass behavior. Studies of defective ZFO are even scarce. We can cite the work of Jinhuan Yao *et al*. [48] that reported the effect of Zn-, Fe- and O-vacancies on the structural and electronic properties of ZFO.

As a conclusion, the knowledge of the structure of ZFO at the microscopic level is limited and the spin configuration of ZFO remains unclear. Other open question is whether the ferrimagnetic response of ZFO can be attributed to the inversion degree or also to defects such as oxygen vacancies and how the cation inversion (antisites) is influenced by an oxygen vacancy. In order to unravel these questions, in this work we will present an *ab initio* study of the role of defects (oxygen vacancies and antisites) on the structural, electronic, magnetic and hyperfine properties of bulk ZFO. We will study the relationship between magnetic response and the type and concentration of defects, showing that cationic inversion and oxygen vacancies play a fundamental role in the origin of ferromagnetic regions in ZFO, giving rise to a ferrimagnetic response of the system.

This paper is organized as follows. In section 2 we will present the detail of the calculation method. In section 3 we will discuss our results for the defective (reduced) system $ZnFe_2O_{4-\delta}$. In section 4 the effect of cationic inversion on the structural, electronic and magnetic properties of ZFO considering different inversion-degrees will be presented. In section 5 the effect of combined oxygen vacancies and cationic inversion will be discussed. Finally, in section 6 the conclusions will be presented.

2. The system under study, computational method and hyperfine parameters.

ZFO ferrite crystallize in a face-centered cubic lattice with a close-packed arrangement of oxygen ions (spinel structure, space group *Fd3m* (*Oh7*)), with Zn and Fe ions at two different crystallographic sites (sites *A* and *B*, Ref. 49). These *A* and *B* sites have O_4 (tetrahedral) and O_6 (octahedral) oxygen coordination, respectively. ZFO adopts the normal spinel structure. In this normal structure the Zn atoms are located at tetrahedral *A*-sites (Wyckoff position 8*a* (1/8, 1/8, 1/8)), whereas the Fe atoms (which carries a magnetic moment due to the partially filled 3*d* shell) occupy the octahedral *B*-sites (16*d*, (1/2, 1/2, 1/2)). The O atoms are at 32*e* (*u,u,u*) positions of the *f.c.c.* structure (*u*= 0.258 [50] for the -3*m* origin). Different values of the lattice parameter *a* have been reported for ZFO ranging from 8.43 to 8.46 Å [23, 50-53]. The Fe-O and Zn-O bond lengths are 2.04 and 2.00 Å, respectively.

Our goal here is to calculate the structural, electronic, magnetic and hyperfine properties of ZFO within density functional theory (DFT, 54-56). For the exchange and correlation functional we employed the Wu–Cohen parameterization of the generalized gradient approximation (GGA) [57]. To better describe the 3*d*-levels of Fe and Zn a Hubbard *U* term (GGA+*U*) in the self-interaction correction (SIC) scheme was included [58]. In this study we took *U*=5 eV for the3*d*-Fe and 3*d*-Zn orbitals [47].

For solving the scalar-relativistic Kohn–Sham equations, we have used the augmented plane waves+local orbital (LAPW+lo) method [56, 59, 60] as implementedin the WIEN2K package [61]. In this method, the wave-functions are expanded in spherical harmonics inside non-overlapping atomic spheres (muffin-tin spheres) of radius R_{MT} and in plane-waves in the remaining space of the unit cell (the interstitial region). The R_{MT} used for Zn and Fe were 1.06 Å and for the oxygen atoms the R_{MT} value employed were 0.8 Å. The plane wave expansion of the wave function in the interstitial region was truncated at $K_{max}=7/R^{min}_{MT}$ (R^{min}_{MT} is the minimum muffin-tin radius). We introduced local orbitals to better describe O-2*s*, Fe-3*p* and Zn-3*p* orbitals [61]. A very-well converged *k*-mesh of 50 *k*-points in the irreducible part of Brillouin zone was used. In all cases, atomic positions were relaxed until the forces were below 1meV/Å.

By examining the effect of different basis sets and k-point samplings we conclude that for $K_{max}=7/R^{min}_{MT}$ and 50 k-points numerical errors are negligible and our results are converged in 2% or less, giving confidence to our conclusions. In particular, energies differences are converged in the order of 1meV per unit formula (for a detailed description of our convergence tests see Ref. 47).

Similar to the case of pristine ZFO reported in Ref. 47, we have considered in our study several spin configurations that include the ferromagnetic case, different antiferromagnetic spin arrangements and some ferrimagnetic configurations. Most of these magnetic configurations present a symmetry that is smaller than the crystal space group. For these reason a cubic super-cell (SC) that contains 56 atoms was constructed from the 14-atoms primitive cell in order to describe all the magnetic structures. These spin configurations are listed in Table 1. The spin arrangement called AF1 is formed by spin chains with two orientations crossing each other along the lattice. The second structure (AF2 in the following) consists of a pair of spins aligned ferromagnetically but antiferromagnetically to another pair from the nearest layer. The other spin-arrangements (AF3, AF4, AF5) consist of random distributions of 8 Fe atoms with positive spins and 8 Fe atoms with negative spins in the 16 B sites of the structure.

To conclude this section, we briefly resume the calculation of the hyperfine parameters of interest for this work. Nuclear techniques, such as Mössbauer Spectroscopy (MS),have the "ability" to measure charge-symmetry related properties, such as the electric field gradient (EFG) tensor, as well as magnetic properties, such as magnetic hyperfine fields (*BHF*), making it possible to obtain a characterization of the electronic and magnetic configuration near and at the probe nucleus [62, 63]. In this work we will compared our calculations with three experimentally determined parameters: the isomer shift (*IS*), which provides information on the local chemical bond, the quadrupole splitting (*QS*), which is a "fingerprint" of the local symmetry around the probe nucleus and the *BHF*, an observable that is directly related to the magnetic configuration and the spin polarization near and at the probe nucleus. The *IS* is given by [62, 63]:

$$IS = \alpha(\rho_A - \rho_R) \qquad (1)$$

where ρ_A and ρ_R stand for the electron charge densities at the nuclear positions in two different solid state environments, the absorber (A) and the reference (R, $B.C.C.$-Fe), respectively. α is a calibration constant with a value 0.27 a.u.^{3}/mms for the 14 keV excited state of ^{57}Fe [47].

The QS is originated by the interaction of the nuclear quadrupole moment with the crystalline electrostatic potential. For the case of the $I=3/2$, 14.4 KeV excited state of ^{57}Fe, the QS is given by [62, 63]:

$$QS = \frac{eQ}{2} V_{ZZ} \left(1 + \frac{\eta^2}{3}\right)^{1/2} \quad , \qquad (2)$$

being:

$$\eta = \frac{V_{XX} - V_{YY}}{V_{ZZ}} \qquad (3)$$

the asymmetry parameter. In the above equations e is the elementary charge and Q is the nuclear quadrupole moment of the 14 keV excited state of the ^{57}Fe Mössbauer-probe nucleus [62]. V_{XX}, V_{YY} and V_{ZZ} are the principal components of the diagonal EFG tensor in a coordinate system with the convention $|V_{XX}| \leq |V_{YY}| \leq |V_{ZZ}|$, being Vii the second derivative (with respect to the spatial coordinates) of the Coulomb potential $V(r)$ created by the charge density surrounding a given nucleus. The V_{ii} components can be determined straightforwardly once the total charge distribution has been accurately calculated.

Finally, the BHF will be calculated using the model proposed by Novak and Chlan [64]. In this model, the spin magnetic moments of the Fe-3d (μ_{3d}) and the Fe-4s (μ_{4s}) electrons are obtained and BHF is expressed as their linear combination:

$$BHF = a\,\mu_{3d} + b\,\mu_{4s} \qquad (4)$$

With a=16.92 T/μ_B and b=1229 T/μ_B [64].

3. Results.

3.1. Pristine ZFO.

Initially, for a simple comparison with the results that we will discuss in the next sections, we will briefly report the results obtained for bulk ZFO. For a detailed discussion of these results see Ref. 47.

For pristine ZFO, the lowest energy configuration corresponds to the antiferromagnetic configuration AF2 (see Table 1) [47]. For this arrangement our calculations predict a=8.46 Å, u=0.260, a band gap in the order 2.0 eV and magnetic moments at the Fe sites, μ(Fe), of ±4.20 μ_B (no spin polarization was found at the Zn sites, while the magnetic moment at the oxygen atoms is smaller than ±0.05 μ_B). These theoretical results are in excellent agreement with the experimental ones (see Refs. 23, 50-53, 65). Concerning the hyperfine parameters, the LAPW+lo calculations predict that all the antiferromagnetic configurations present similar hyperfine parameters (*BHF* in the order of 51 T, *IS* of 0.38 mm/s and *QS* in the order of 0.20-0.24 mm/s). For the ferromagnetic configuration, a smaller *BHF* is predicted by LAPW+lo (48.5 T) and a larger *QS* value (0.28 mm/s). The *IS* value is 0.39 mm/s. These results are in excellent agreement with the experimental ones [23, 47]. All these results will be the base-line in our study of the role of the defects in the different properties of ZFO. For all the magnetic configurations the energy required to flip one spin resulted to be $\Delta E = E^{AFi} - E^{flip} = $ -10 meV/formula unit (*f.u.*), being E^{AFi} the energy of a given antiferromagnetic configuration.

3.2. Oxygen vacancies (ZnFe$_2$O$_{4-\delta}$).

In order to study how an oxygen vacancy affect the structural, magnetic and hyperfine properties of ZFO and the role that it plays in the magnetic response of the system we use the 56 atoms SC´s previously described removing an oxygen atom (δ=0.125, a vacancy concentration

of 3%) and taking into account the volume changes and the structural distortions induced by the oxygen vacancy.

From the study of the total energy as a function of the lattice constant a (see Fig. 1) we found that the lowest energy states correspond to the antiferromagnetic cases and, for all antiferromagnetic configurations studied here, the lowest energy corresponds to the AF2 spin arrangement. As can be seen in Table 2, the energy differences between configurations AF2, AF3, AF4 and AF5 (that also consist of parallel spin clusters) are very small, close to our convergence error. This result show that the energy landscape of reduced ZFO is, similar to the results found for stoichiometric ZFO, complex and characterized by a number of very closed local energy minima,

Independently of the spin configuration considered, the oxygen vacancy induces a small enlargement of the volume cell (the lattice parameter is increased from 8.46 Å for the pristine system to 8.47 Å for the reduced case. Differences in the a values for the different spin configurations are smaller than the precision error). This result is in clear contradiction with those obtained by J. Yao *et al.* [48], who predicted a=8.204 Å. This result raises many doubts, since the same authors and using the same method of calculations reports a=8.274 Å for pristine ZFO [66], in very bad agreement with the experimental results [23, 49-53]. We have to mention here that in both works the authors employed a pseudopotential method in the framework of the GGA approximation. It is well-known that the exchangeand correlation effects included in GGA are insufficient to describe 3-d transition oxides and in ZFO ferrite in particular [47], Also spin-polarization was not considered by J. Yao *et al.* in their calculations.

The oxygen vacancy also induces a strong structural relaxation of the atomic positions in the SC. Due to the highly ionic character of the ZFO crystal, the Fe nearest neighbors to the vacancy site repel each other and leave a big "hole" in the place of the vacancy. Depending on the spin arrangement, these Fe atoms are displaced as much as 0.15 Å away from their original positions. Particularly, for the AF2 configuration the distance Fe-vacancy site are enlarged from 2.04 Å to 2.10 Å (for two of the Fe neighbors, Fe1 and Fe2 in Fig. 2) and 2.13 Å (for the third one, Fe3 in Fig. 2). The next-nearest Fe atom (Fe4), originally located at 3.53 Å, is essentially

not affected by the presence of the oxygen vacancy (after the structural relaxation, the vacancy site distance is 3.54 Å).

After the determination of the lower energy configuration, we can discuss the results for electronic and magnetic properties. Initially, we study the stability of ZFO with an O-vacancy through the vacancy formation energy (E^{vac}) defined as:

$$E^{vac} = E^{AF2+vac} - E^{AF2} + \mu(O)$$

where $E^{AF2+vac}$ and E^{AF2} are the total energies of the AF2 configuration with one oxygen vacancy and stoichiometric ZFO respectively and $\mu(O)$ is the chemical potential of the oxygen atom. Assuming that $\mu(O)$ is the half of the total energy of an oxygen molecule (calculated with the same precision that the energy of stoichiometric and reduced ZFO), the vacancy formation energy resulted to be +7.8eV, indicating that O-vacancy in ZFO cannot be formed spontaneously. However, depending on the method and growth conditions of the sample [5, 7, 38, 39, and references therein], physical conditions can induce the formation of reduced ZFO.

At this point, we study the possibility to flip one spin but now in presence of an oxygen vacancy. To do this, total energies calculations were performed flipping the spin of one Fe atom of the SC from positive to negative (or negative to positive) for the different spin configurations. We found that the flip is more favorable (less energy required) in the case of the spin configuration AF2 and when Fe1 or Fe2 atoms are changed from positive to negative. For this new spin arrangement (FERRI3 in the following) all the magnetic moments are the same, with the exception of Fe1 that changes from +4.0 μ_B to -4.0 μ_B, giving raises to a cell with a lattice parameter a=8.47 Å, a net magnetic moment of -8.0 μ_B (0.5 μ_B/Fe atom in the cell) and a region with three spin with parallel alignment, see Fig. 2. It is important to note that the energy difference $\Delta E = E^{AF2} - E^{FERRI3}$ is -1 meV/$u.f.$(see Table 2). This energy difference is in the order of our convergence error, so the AF2 and the FERRI3 configurations can be considered as degenerate solutions. In consequence, the lowest energy configuration of reduced ZFO could be antiferromagnetic or ferrimagnetic. This result is in agreement with the experimental ones reported by Rodríguez Torres et al. [5] who demonstrated (by means of XMCD and

magnetization measurements) the relevance of oxygen vacancies in the formation of local ferromagnetic coupling between Fe ions at octahedral sites in zinc ferrites thin films. This coupling gives rise to a ferrimagnetic ordering with a Curie temperature above 300 K. Our results are also in agreement with experimental and theoretical works [44, 45, 67] that probed that an adequate concentration and distribution of oxygen vacancies could play a fundamental role in the magnetic response of otherwise non-magnetic oxides.

The oxygen vacancy also produces changes in the electronic populations in the Fe muffin-tin spheres. Based in a Bader analysis [68] we found that the oxygen vacancy induces an increment in the charge in its Fe nearest neighbors. For the case of the lowest energy configurations (AF2 and FERI3) the charge in the muffin-tin spheres of Fe1 and Fe2 increase from $23.695e$ to $23.766e$. For Fe3, the charge in its muffin-tin spheres is $23.903e$ (the charge of the other atoms of the SC remains unaltered). These changes are reflected in the Fe-magnetic moments. For the case of the Fe atoms close to the vacancy, magnetic moments of $+4.0$ μ_B (Fe1 and Fe2) and -3.6 μ_B (Fe3) were found. All the other Fe atoms of the cell present magnetic moments of ±4.2 μ_B, as in the case of the stoichiometric structure. Additionally, spin polarization in the order of ±0.1 μ_B at the O sites is predicted (the Zn atoms remains non-polarized). These changes in the magnetic moments of the Fe atoms close to the vacancy site are also predicted for the other antiferromagnetic and the ferromagnetic configurations studied here.

The changes in the band structure of ZFO induced by the oxygen vacancy can be visualized in the density of states (DOS) presented in Fig. 3. The formation of an oxygen vacancy produce a displacement of the Fermi level towards the conduction band and partially occupied vacancy-levels appears in the band gap of ZFO. These states have mainly Fe1-, Fe2- and Fe3-$3d$ and O-$2p$ character, and are spatially located at these atoms.

The structural and electronic changes induced by an oxygen vacancy in ZFO will be also reflected in the hyperfine parameters at the Fe sites, magnitudes that can be directly measured in MS experiments. The comparison of experimental results and *ab-intio* calculated hyperfine parameters can be used to determine the local structure around a probe site (Fe in the present case), as it was demonstrated in Ref. [69]. In Fig. 4 we present our predictions for the *IS*,

QS and *BHF* at the Fe sites of the 56-atoms SC of $ZnFe_2O_{4-\delta}$ obtained for the lowest energy spin configurations, i.e., AF2 and FERRI3. For the case of the configuration AF2, the *IS* at two of the three Fe atoms neighbors of the oxygen vacancy (Fe1 and Fe2) increases up to 0.47 mm/s and the *IS* at the other neighbor (Fe3 site) grows up to 0.87 mm/s. This changes in the *IS* indicates a transition from Fe^{+3} to Fe^{+2} oxidation state, in agreement with the increment in the electronic charge of the Fe atoms that surrounds the vacancy site. Similar results were obtained for the configuration FERRI3, but in this case the *IS* at the Fe1 site is also in the order of 0.87 mm/s. In consequence, the effect of the oxygen vacancy is to increase the average *IS* to 0.44 mm/s (0.40 mm/s for the pristine structure). In the case of the *BHF*, for both AF2 and FERRI3 spin configurations the formation of an oxygen vacancy induce a reduction in the magnitude of the hyperfine field at the sites Fe1, Fe2, and Fe3, while for the other Fe sites (far away from the oxygen vacancy site) the *BHF* is very similar to those predicted for the pristine structure (see Fig. 4). As a consequence of the presence of the oxygen vacancy, and the structural and electronic distortion induced by it, an increment of the *QS* at the Fe atoms nearest neighbours of the vacancy site is predicted (see Fig. 4) for both AF2 and FERRI3 spin configurations.The *QS* for the Fe atoms far away from the oxygen vacancy are similar to those predicted for the pristine system, being the average value of the *QS*= 0.25 mm/s.

Resuming, the overall, effect of an oxygen vacancy in the hyperfine properties at the Fe sites of reduced ZFO is to increase the average values of the *IS* and *QS*, and a reduction of the average *BHF* value. These conclusions were obtained for the case of one vacancy in the SC. When more than one oxygen vacancy in the SC is considered, the average *IS*, *BHF* and *QS* will depend on the concentration and distribution of vacancies in the cell, but calculations performed including two oxygen vacancies and different locations in the SC reveals that the general conclusions presented here are still valid.

Finally, we also study the case of two oxygen vacancies in the supercell (δ =0.25). We found that the oxygen vacancies repel each other, being the lowest energy configuration those that corresponds to one oxygen vacancy far away from the other. None of the conclusions obtained for δ=0.125 are modified when this second oxygen vacancies is introduced. Lattice

parameters, the DOS, and the magnetic moments follows the same trends previously discussed. Concerning the magnetic ordering, a ferrimagnetic spin arrangement in which one Fe atom close to one of the oxygen vacancy and one Fe atom close to the second one change it spin orientations have an energy that differs in about 1 meV/$u.f$ from those of ANTI2 (degenerate solutions). This ferrimagnteic configuration has a net magnetic moment of 15.0 μ_B per unit cell (0.95 μ_B/Fe atom).

3.3. Antisites (cationic inversion), $(Zn_{1-\alpha}Fe_\alpha)[Zn_\alpha Fe_{2-\alpha}]O_4$.

The second defect studied was the antisites (cationic inversion), that consists in the swapping between Fe and Zn atoms, as shown Fig. 5. Partially inverted ferrites can be described as $(M_{1-\alpha}Fe_\alpha)[M_\alpha Fe_{2-\alpha}]O_4$ where round and square brackets denote A and B sites, respectively and α is the inversion parameter. α=0 correspond to a normal ferrite, α=1 to inverted ferrites and intermediate values of α corresponds to partially inverted systems.

We study here the two limit cases: α=0.125 (partially inverted ZFO, one Fe at A-site and one Zn at the B-site) and α=1 (inverted ZFO, the 8 sites A occupied by Fe atoms and 8 Fe and 8 Zn atoms at the B sites). In both cases, different questions must be answer prior to any discussion. For the partial inversion case (α=0.125) first question concerns the preferred distance between the Fe and Zn atoms involved in the inversion. So we perform calculations swapping one Zn atom with one of it first neighbor Fe atom (Fe-Zn distance of 3.5 Å) and secondly we swap one Fe atoms and one Zn atom that are far away each other. Total energy calculations indicated that the lower energy correspond to the case in which one Fe atom is swapped with one of its Zn nearest-neighbours. We will use this configuration in the following studies of partially inverted ZFO.

The second question is the spin orientation of the Fe atom at the A site. So, we performed calculations considering the AF2 spin configuration and two possible scenarios:

i)   One Fe atom with positive spin is swapped with a Zn atom keeping its original spin orientation, see Fig. 5b.

ii)   Same as i), but now the spin orientation of the Fe atom located at the *A*-site is changed to negative.

In case i), the magnetic moment of the Fe atom at the *A*-site (Fe^A) is +4.2 μ_B, the same value that we obtained for Fe at the *B*-sites in the pristine structure. The Fe atoms that remain at the *B*-sites present magnetic moments of +4.2 μ_B (seven Fe atoms) and -4.2 μ_B (eight Fe atoms). O atoms, the Zn atoms at *A*-site and the Zn atom located at the *B*-site (Zn^B) are not spin-polarized. In consequence, the total magnetic moment of the cell is null and the system is still antiferromagnetic. However, as we will discuss below, the inversion promotes the flip of other Fe in *B* site then, a ferrimagnetic configuration will has the lower energy. In case ii), the predicted value of the magnetic moment of Fe^A is -4.2 μ_B. The magnetic moments of the Fe atoms that remain at the *B*-sites, the O atoms and the Zn atoms are not affected by the change in the spin orientation of Fe^A. In consequence, the resulting system is ferrimagnetic (a net magnetic moment of -8.5 μ_B per unit cell). Comparing energies of cases i) and ii) we found that the lowest energy corresponds to the antiferromagnetic system (case i).

In the case of the inverted system, all the 8 *A*-sites of the structure are occupied by Fe atoms and 8 Fe and 8 Zn occupies the 16 *B*-sites of the SC. The question that appears here is the distribution of the Fe and Zn atoms in these 16 sites. From the study of different distributions we conclude that the lowest energy structure correspond to the case in which the 8 Fe with spin + in Table 1, AF2 configuration, are swapped with the Zn atoms, the 8 Fe atoms with spin - remains in its sites and the Zn atoms occupy the remaining *B*-sites. For this structure, the magnetic moments of Fe at A- and *B*-sites are +4.2 μ_B and -4.2 μ_B, respectively, and therefore the net magnetic moment of the cell is null.

After these previous studies, we can discuss the effect of antisites on the different properties and the magnetic response of ZFO. The equilibrium lattice parameter *a* for the partially inverted and the inverted structures were found to be 8.45 and 8.44 Å, respectively, see Fig. 6. These

results imply that inversion induce a small volume reduction when comparing to the normal case (a=8.46 Å). This reduction of the volume cell as a function of the increasing inversion degree is in perfect agreement with the results reported by M. Niyaifar [70], who found that when the inversion degree increases from α=0.0375 to α=0.16, the lattice parameters diminishes from 8.452 Å to 844 Å. Also, the antisite induces local geometrical distortions in the O_{NN} coordination-spheres of Fe^A and Zn^B (the magnitude of the structural distortions rapidly decreases for atoms located beyond the O_{NN} spheres of Fe^A and Zn^B). Fe^A induces a contraction of the Fe-O_{NN} bond-lengths. On the other hand, Zn^B induces an enlargement of the Zn-O_{NN}, see Table 3. The magnitudes of these structural distortions are nearly independent of the degree of inversion, and properties like magnetic moments or charge in the atomic spheres are nearly independent of the structural distortions.

An important result is that the normal structure has lower energy than the inverted or the partially inverted ones (see Fig. 6), in agreement with the literature that affirms that ZFO is a normal spinel [10]. By comparison of the energies of the normal and partially inverted structures we can obtain that 85 meV/$u.f.$ is the energy necessary to exchange a Fe atom with one of its Zn neighbors.

With these results, we return to the ferromagnetic and the five antiferromagnetic configurations. In Table 4 we present the results obtained for the energy of each spin arrangement for the partially inverted structure. As in the other cases previously studied, the lowest energy configuration corresponds to the AF2 one, but now AF3, AF4, AF5 and AF2 differs in less than 3 meV/$u.f.$, an energy difference that is close to our precision error. Similar results were obtained for the case of the inverted structure. Similar to the previous cases, we also study the energy necessary to flip one spin from positive to negative (or from negative to positive), flipping the spin of different Fe atoms. From these studies we found that the lowest energy case corresponds to the flip of a Fe spin (initially with positive spin, Fe5 in Fig. 5) that is a first next nearest neighbor of the Fe^A atom (Fe^A-Fe5 distance of 3.53 Å). When the spin of Fe5 is flipped, the magnetic moment of Fe5 changes from +4.2 μ_B to -4.2 μ_B and the resulting system (that we will call FERRI4) has a lattice parameter of 8.45 Å and a net magnetic moment of -10.0

μ_B per unit cell (0.62 μ_B/Fe atom). More interesting, the energy difference $\Delta E = E^{AF2} - E^{FERRI4}$ is +6 meV/$u.f.$, see Table 4. This positive energy difference implies that the solution with a net magnetic moment is energetically favorable. In this spin arrangement a cluster of three Fe atoms with parallel spins is formed, showing that the inversion (even a small degree of inversion) could play a fundamental role in the ferrimagnetic response of ZFO as it was suggested in Ref. 41.

We can understand the preference of Fe5 atom to change its spin from positive to negative with a simple model for the super-exchange interaction. Fe^A and Fe5 present parallel alignment in the AF2 configuration and both atoms are linked by an oxygen atom, forming a Fe^A-O-Fe5 path. The bond-lengths Fe^A-O and Fe5-O are 1.98 and 2.01 Å, respectively, and forms an angle of 130º. In this geometric configuration the favorable configuration of both Fe is antiparallel [26, 71] and in consequence the system reaches the lowest energy when one of the Fe atoms change its spin orientation.

In Fig. 7 we present the DOS of partially inverted and inverted ZFO. As can be seen, the system is still a semiconductor upon inversion, but the band gap is reduced to 2.1 eV (a reduction of 0.1 eV comparing with the pristine case). All the general features of the DOS are very similar to those previously discussed for pristine ZFO [47] and are nearly independent of the spin configuration.

Concerning the hyperfine parameters, the IS at the 15 Fe-atoms located at B-sites is the same that those of pristine ZFO (0.38 mm/s), while Fe^A present a smaller IS (0.30 mm/s), see Fig. 8. This result (IS for Fe atoms at sites A 0.08 mm/s smaller than that of Fe atoms at sites B) does not depend on the inversion degree and neither the spin configuration. This means that the average IS over the entire 56-atoms SC will be 0.375 mm/s in the case of one inversion or 0.34 mm/s in the case of the inverted ZFO. Similarly, the BHF at Fe atoms located at B-sites is very similar to those obtained for pristine ZFO, while BHF at Fe^A is 2 T smaller (see Fig. 8). In the case of the QS, Fe^A is characterized by QS^A=0.23 mm/s while a QS distribution was found for Fe at sites B, with an average QS of 0.33 mm/s and width of 0.09 mm/s.

At this point, we can compare our predicted results with experimental ones. Lima *et. al.* [72] and Isfahani *et al.* [73] and performed MS experiments at 4K in ZFO nanoparticles. By applying an external magnetic field the contributions of Fe located at both cationic sites could be resolved. As can be seen in Table 5, our *ab initio* predictions for the *IS* and *BHF* are in excellent agreement with the experimental results. We can also compare our *ab initio* predictions with MS experiments performed at 300 K using ZFO nanoparticles samples with a known degree of inversion [70]. Experimental results at 300 K can only be crudely compared with the *ab initio* predictions (that correspond to 0 K) because all possible thermal effects are not included in the calculations. From the experimental side, at 300 K is not possible to resolve the contribution of each site to the spectra. In consequence, the MS results consist of one doublet originating from a quadrupole interaction. The average QS and IS values obtained for each sample are reported in Table 6. From this Table we can see that the effect of the inversion in the hyperfine parameters that our *ab initio* predictions is good agreement with the experimental results. Due to the extreme sensitivity of the hyperfine interactions to small changes in the electronic and magnetic structure of the system under consideration, the agreement theory-experiment for the *IS*, the *QS* and the *BHF* gives confidence to the results of our study of defective ZFO.

3.4. Oxygen vacancies and antisites, $(Zn_{1-\alpha}Fe_{\alpha})[Zn_{\alpha}Fe_{2-\alpha}]O_{4-\delta}$

In previous sections we study the effect on the magnetic response and different properties of ZFO of the oxygen vacancies and antisites separately. Now, we will consider both defects in conjunction. In this case, the calculations were performed considering the presence of a single oxygen vacancy (δ=0.125) and the partially inverted system (α=0.125). Based in the previous results we considered the inversion process involving Fe and Zn atoms that are first neighbors (Fe-Zn separation distance of 3.50 Å), keeping the original spin orientation for Fe^A. However, an important question must be resolved, the vacancy site location in the partially inverted structure. Accordingly, different positions for the oxygen vacancy in the structure were

considered. By comparing the total energy for the different oxygen vacancy locations we identify the most stable site for it, that corresponds to an oxygen vacancy site that is first neighbor to Zn^B and not first neighbor of Fe^A, see Fig. 9 (distance oxygen vacancy site-Fe^A= 3.45 Å). This preferential site for the oxygen vacancy can be understood in the framework of a simple ionic model. Zn presents a +2 oxidation state. When Zn is exchanged with a Fe^{+3} to a site with a six-fold O_{NN} coordination, a vacancy is required to compensate charge. On the other hand, the Fe presents oxidation states 2+ and 3+, so when replacing a Zn^{2+} no charge unbalance at the defect site occurs.

From the study of the different spin configurations reported in Table 1 we found that the lowest energy spin configuration is the AF2 one (see Table 7) with $a = 8.48$ Å (a value that is nearly independent of the spin configuration). In consequence, the oxygen vacancy and the partial inversion induce a small increase in a with respect to the pristine structure ($a = 8.46$ Å). In addition, and as can be seen in fig. 10, reduced ZFO with normal structure has lower energy than the reduced and partially inverted system. However, the energy difference between these structures is now 32 meV/$u.f.$ This difference in energy is smaller than the energy required for the inversion process without oxygen vacancies (85 meV/$u.f.$), so we predict that reduced ZFO will have a larger inversion degree than the stoichiometric system. Similarly, the formation energy of one oxygen vacancy resulted to be (in presence of cationic inversion) 7.4 eV, which is a value slightly lower than those found in the normal structure (7.8 eV).

Now we will centre our attention in the ferrimagnetic solutions, studying the energy necessary to flip one Fe-spin in presence of inversion and oxygen vacancies. Based in the previous results we also considered the inversion of the spin of both Fe1 (Fe atom that is a first neighbour of the vacancy site) and Fe5 (next-nearest neighbour of Fe^A) atoms. Interestingly, our calculations predict that when the spin of these two atoms are inverted the resulting ferrimagnetic system (FERRI5) have a net magnetic moment of 20.0 μ_B per unit cell (1.25 μ_B/Fe atom) and its energy is -62 meV/$u.f.$ In consequence FERRI5 is clearly the lowest energy configuration of $(Zn_{1-\alpha}Fe_{\alpha})[Zn_{\alpha}Fe_{2-\alpha}]O_{4-\delta}$. Consequently, samples grown in reducing atmosphere, in which the number of oxygen vacancies is increased, will have more cationic inversion than

samples grown in oxygen-rich atmospheres and therefore the magnetic response of the samples will be different, being the ferrimagnetic response favored in accordance with the experimental findings reported in Refs. 5, 38, 40, and 41. Also, our results are in agreement with those reported in Ref. 24 that suggest that the long-range order in ZFO is driven by defects and quenched atomic disorder.

Regarding electronic and magnetic properties, we found that the magnetic moments of the two Fe atoms first neighbors to the vacancy site (Fe1 and Fe3. Fe2 is now located at the A site) present magnetic moments lower (-3.6 and +3.6 μ_B, respectively) than those of the other 14 Fe atoms of the structure (± 4.2 μ_B). In addition, some of the oxygen atoms in this reduced and partially inverted system present a polarization of 0.1 μ_B. Consequently, none of the results discussed in the previous sections (when both defects were treated separately) changes when both structural defects are treated jointly.

Fig. 11 shows the DOS of $(Zn_{1-\alpha}Fe_\alpha)[Zn_\alpha Fe_{2-\alpha}]O_{4-\delta}$. Comparison of Fig. 3, 7 and 11 shows that the effects induced by the oxygen vacancy and cationic inversion appears here: vacancy levels in the band-gap and the Fermi level is shifted to the conduction band and the gap between the filled O-2p and the empty Fe-3d band is reduced in about 0.2 eV.

Finally, the *ab initio* predictions for the hyperfine parameters at the Fe sites of $(Zn_{1-\alpha}Fe_\alpha)[Zn_\alpha Fe_{2-\alpha}]O_{4-\delta}$ are shown in the Fig. 12. Here we can see that the *IS* at the Fe sites that are close to the vacancy site (Fe1 and Fe3) increases it value to 0.87 mm/s, which is in accordance with the already discussed transition from Fe^{3+} to Fe^{2+} of these atoms. On the other hand, the *IS* at Fe^A site decreases to 0.30 mm/s, as occurs in the stoichiometric partially inverted structure. For the other Fe atoms, the *IS* value is very similar to that obtained for the pristine structure (0.38 mm/s). This behavior is very similar for all antiferromagnetic and the FERRI5 configurations. In the case of the *QS* (see Fig. 12) it presents a value of 2.45 mm/s in the case of Fe1 and Fe3 sites, while for the Fe^A site *QS*=0.24 mm/s is predicted. For the other Fe atoms that remains is the *B*-sites of the structure, a distribution of *QS* values (originated by the structural and electronic distortion induced by the oxygen vacancy and the antisite) with a centroid of 0.32 mm/s and a width distribution of 0.07 mm/s was found. Therefore, the effect of oxygen

vacancies and inversion is to increase the magnitude of the average *QS* value. Finally, *BHF* at the sites Fe1, Fe3 and Fe^A decreases its magnitude see Fig. 13, while the Fe atoms located at the *B*-sites present *BHF* values that are very similar to that obtained for the pristine structure of ZFO (51.1 T). Consequently, the average value of the *BHF* for the structure with vacancies and inversion decreases to 49.6 T. In summary, the effect of oxygen vacancies and cationic inversion (when are considered together) in the hyperfine ZFO properties to increase the *IS* and the *QS* and to reduce the average *BHF*, in agreement with the experimental results reported in Ref. 69.

4. Conclusions.

In the present work we have studied by means of *ab initio* GGA+*U* calculations the structural and electronic properties of reduced, partially inverted and partially inverted and reduced ZFO. The hyperfine parameters at the Fe sites for different spin arrangements (ferromagnetic and different ferromagnetic and antiferromgnetic configurations) were determined.

We study the effect of cationic inversion and oxygen vacancies on the cell-volume and the internal atomic positions, characterizing the local structure around the Fe-sites in each case. Concerning electronic properties we found that the oxygen vacancy induces the formation of levels at the Fermi level. Inverted ZFO presents a semiconducting nature with a band-gap 10% smaller than normal ZFO. This band-gap reduction slightly depends on the inversion degree.

The hyperfine parameters (isomer shift, quadrupole splitting and hyperfine fields) reported by MS experiments at 300 and a 4 K are successfully reproduced by our calculations, enabling us to characterize the electronic and magnetic structure around the Fe-sites. Since the hyperfine parameters are very sensitive to fine details of the electronic and magnetic structure around the Fe-probes, these result gives confidence to our study.

Our calculations predict that, when defect are introduced in ZFO ferrimagnetic solutions have lower energies than the antiferromagnetic ones. In these cases, net magnetic moments of

0.5 μ_B/Fe (reduced ZFO), 0.625 μ_B/Fe (partially inverted ZFO) and 1.25 μ_B/Fe (ZFO with one oxygen vacancy and partially inverted) are predicted. These results are in agreement with the experimental ones that show that samples with defects present net magnetic moments and high ordering temperatures (ferrimagnetic behavior) while a null magnetic moment is reported for pristine and normal ZFO. Now, our calculations enable us to discriminate the role played by each defect in the origin of the observed ferromagnetic response of defective $ZnFe_2O_4$.

An important result obtained here is that the energy necessary to produce cationic inversion in reduced ZFO is smaller than in the stoichiometric system. In consequence, we predict that samples grown in reducing atmosphere will have a higher degree of cationic inversion than samples grown in oxygen-rich atmospheres. Since the magnetic properties of ferrites strongly depend on the cation distribution in both cationic sites of the structure, the magnetic response of the samples grown in reduced or oxidant atmospheres will be different. In particular we probe that both oxygen vacancies and antisites (cationic inversion) play a fundamental role in the formation of local ferromagnetic coupling between Fe ions, giving rise to a ferrimagnetic ordering in an otherwise antiferromagnetic compound, in accordance with the experimental findings obtained by means of x-ray magnetic circular dichroism and magnetization measurements performed on zinc ferrites with different cation distributions and oxygen vacancy concentrations reported in the literature. So, the ferrimagnetic response observed ZFO thin films or ZFO nanoparticles can betaken as a further example of defect-induced magnetism.

Bibliography

[1] H. Ohno, Making nonmagnetic semiconductors ferromagnetic, Science **281** (1998), 951.

[2] J. F. Gregg, Spintronics: A growing science, Nature Materials **6** (2007), 798.

[3] H. Ohno, M;. D. Stiles, and B. Dieny, Spintronics, Proceedings of the IEEE 104 (2016), 1782.

[4] Chao Jin, Peng Li, WenboMi, and HailiBai, Structure, magnetic, and transport properties of epitaxial $ZnFe_2O_4$ films: An experimental and first-principles study, J. Applied Phys. 115 (2014), 213908.

[5] C.E. Rodríguez Torres, G. A. Pasquevich, P. M. Zélis, F. Golmar, S. P. Heluani, S. K. Nayak, W.A. Adeagbo, W. Hergert, M. Hoffmann, A. Ernst, P. Esquinazi, S. J. Stewart, Oxygen-vacancy-induced local ferromagnetism as a drivingmechanism in enhancing the magnetic response of ferrites, Phys. Rev. B 89(2014), 104411.

[6] K. E. Sickafus and J. M. Wills, Structure of Spinel, J. Am. Ceram. Soc., **82** (1999), 3279.

[7] Y. Suzuki, Epitaxial spinel ferrite thin films, Annual Rev. Mater.Res. **31**, (2001), 265.

[8] A. Goldman, in Modern Ferrite Technology, 2nd ed. (Springer,Boston, MA, 2006), p. 453.

[9] J. L. G. Fierro, Metal Oxides—Chemistry and Applications (Taylor and Francis, Boca Raton, FL, 2006).

[10] J. Smit, H. P. J. Wijn, in: Ferrites, Philips Technical Library, 1959.

[11] R. E. Vandenberghe and E. De Grave, in Mösbauer Spectroscopy Applied to Inorganic Chemistry, edited by G. J. Long and F. Grandjean ~Plenum, New York, 1989!, Vol. 3.

[12] M. Niyaifar, Effect of preparation on structure and magnetic properties of $ZnFe_2O_4$, J. Magn.19 (2014) 101e105.

[13] S. D. Jackson, Metal Oxide Catalysis (Wiley-VCH Verlag GmbH & Co., Weinheim, 2009), Vol. 2, p. 485.

[14] S. Sun, C. B. Murray, Synthesis of monodisperse cobalt nanocrystals and their assembly into magnetic superlattices, J. Appl. Phys., **85** (199), 4325.

[15] Jinhuan Yao, Yanwie Li, Xuanha Li, Xiaodong Zhu, First-Principles study of thegeometric and electronic structures of zinc ferrite with vacancy defect, Metall.Mater. Trans. A **47** (2016) 3753e3760 and references there in.

[16] Y. F. Chen, D. Spoddig, M. Ziese, Epitaxial thin film $ZnFe_2O_4$: asemi-transparent magnetic semiconductor with high Curie temperature, J.Phys. D: Appl. Phys. **41** (2008), 205004

[17] H. H. Hamdeh, J. C. Ho, S. A. Oliver, R. J. Willey, G. Oliveri, and G. Busca, Magnetic properties of partially-inverted zinc ferrite aerogel powders, J. Appl. Phys. 81 (1997), 1851.

[18] M. Ahmed, L. Alonso, J. M. Palacios, C. Cilleruelo, and J. C. Abanades, Structural changes in zinc ferrites as regenerable sorbents for hot coal gas desulfurization, Solid State Ionics **138** (2000), 51.

[19]J. Liu, G. Lu, H. He, Hua Tan, Tao Xu, K. Xu, Studies on photocatalytic activity of zinc ferrite catalysts synthesized by shock waves.Materials Research Bulletin**31** (1996), 1049.

[20] G. X. Lu, S. B. Li, Hydrogen production by H_2S photodecomposition on $ZnFe_2O_4$ catalyst, Int. J. Hydrogen Energy **17**(1992), 767.

[21] Y. Tamaura, H. Kaneko, Oxygen-releasing step of $ZnFe_2O_4/(ZnO + Fe_3O_4)$-system in air using concentrated solar energy for solar hydrogen production, Sol. Energy **78** (2005), 616.

[22] K. Shetty, L. Renuka, H. P. Nagaswarupa, H. Nagabhushana, K. S. Anantharaju, D. Rangappa, S. C. Prashantha, K. Ashwinie, A comparative study on $CuFe_2O_4$, $ZnFe_2O_4$ and $NiFe_2O_4$: Morphology, Impedance and Photocatalytic studies, Materials Today: Proceedings **4** (2017), 11806.

[23] W. Schiessl, W. Potzel, H. Karzel, M. Steiner, G.M. Kalvius, A. Martin,M.K. Krause, I. Halevy, J. Gal, W. Schäfer, G. Will, M. Hillberg, R. Wäppling,Magnetic properties of the $ZnFe_2O_4$ spinel, Phys. Rev. B 53 (1996) 9143e9151.

[24] K. Kamazawa, Y. Tsunoda, K. Odaka, K. Kohn, Spin liquid state in $ZnFe_2O_4$, J. Phys. Chem. Solids 60 (1999) 1261.

[25] Y. Yamada, K. Kamazawa, Y. Tsunoda, Interspin interactions in $ZnFe_2O_4$: theoretical analysis of neutron scattering study, Phys. Rev. B 66 (2002), 064401.

[26] K. Kamazawa, Y. Tsunoda, H. Kadowaki, K. Kohn, Magnetic neutron scatteringmeasurements on a single crystal of frustrated $ZnFe_2O_4$, Phys. Rev. B 68(2003), 024412 and references there in.

[27] T. Usa, K. Kamazawa, H. Sekiya, S. Nakamura, Y. Tsunoda, K. Kohn, M. Tanaka,Magnetic properties of $ZnFe_2O_4$ as a 3-D geometrical spin frustration system, J. Phys. Soc. Jpn. 73 (2004) 2834e2840.

[28] K. Tomiyazu, K. Kamazawa, A spin molecule model for geometrically frustratedspinel $ZnFe_2O_4$, J. Phys. Soc. Jpn. 80 (2011). SB024-1 SB024-3.

[29] M. A. Hakim, M. Manjurul Haque, M. Huq, P. Nordblad, Spin-glass-like ordering in the spinel $ZnFe_2O_4$ ferrite, Physica B 406 (2011) 48e51.

[30] H. Mamiya, N. Tsujii, N. Terada, S. Nimori, H. Kitazawa, A. Hoshikawa and T. Ishigaki, Slow dynamics in the geometrically frustrated magnet $ZnFe_2O_4$: Universal features of aging phenomena in spin glasses, Phys.Rev. B **90** (2014), 014440.

[31] T. Watanabe, S. Tadataka, K. Tomiyasu, and K. Kamazawa, Acoustic study of dynamical molecular-spin state without magnetic phase transition in spin-frustrated$ZnFe_2O_4$, Phys. Rev. B **92** (2015), 174420.

[32] B. Pandey, F. J. Litterst, E. M. Baggio-Saitovitch, Preferential spin canting in nanosize zinc ferrite, J. Magn. Magn. Mater. **385** (2015) 412e417.

[33] C. B. R. Jesus, E. C. Mendonça, L. S. Silva, W. S. D. Folly, C. T. Meneses, and J.G.S. Duque, Weak ferromagnetic component on the bulk $ZnFe_2O_4$ compound, J. Magn. Magn. Mater. **350** (2014) 47.

[34] J. E. Greedan, Geometrically frustrated magnetic materials, J. Mater. Chem. **11** (2001) 37.

[35] A. P. Ramirez, Strongly geometrically frustrated magnets, Annu. Rev. Mater. Sci. **24** (1994), 453.

[36] S. H. Lee, H. Takagi, D. Louca, M. Matsuda, S. Ji, H. Ueda, Y. Ueda, T. Katsufuji, J. Chung, S. Park, S. Cheong, C. and Broholm, Frustrated Magnetism and Cooperative Phase Transitions in Spinels, J. Phys. Soc. Japan **79** (2010) 011004.

[37] K. Tomiyazu, K. Kamazawa, A spin molecule model for geometrically frustratedspinel $ZnFe_2O_4$, J. Phys. Soc. Jpn. **80** (2011). SB024-1.

[38] K. L. Salcedo Rodríguez, S. J. Stewart, P. M. Mendoza Zélis, G. A. Pasquevich, and C. E. Rodríguez Torres, Role of defects on the magnetic behaviour of the geometrically frustrated spinel $ZnFe_2O_4$, Journal of Alloys and Compounds **752** (2018), 289.

[39] S. Nakashima, K. Fujita, K. Tanaka, K. Hirao, T. Yamamoto, and I. Tanaka, First-principles XANES simulations of spinel zinc ferrite with a disordered cation distribution, Phys. Rev. B **75** (2007), 174443.

[40] J. M. Ramallo López, S. G. Marchetti, J. F. Bengoa, R. J. Prado, F. G. Requejo, S. J. Stewart, and S. J. A. Figueroa. Cationic exchange in nanosized $ZnFe_2O_4$ spinel revealed by experimental and simulated near-edge absorption structure, Phys. Rev. B, **75** (2007), 073408.

[41] S. J. Stewart, S. J. A. Figueroa, M. B. Sturla, R. B. Scorzelli, F. García, and F. G. Requejo, Magnetic $ZnFe_2O_4$nanoferrites studied by X-ray magnetic circular dichroism and Mössbauer spectroscopy, Physica B: Condensed Matter **389** (2007), 155.

[42] S. Ayyappan, S. P. Raja, C. Venkateswaran, J. Philip, and B. Raj, Room temperature ferromagnetism in vacuum annealed $ZnFe_2O_4$ nanoparticles, Appl. Phys. Lett. **96** (2010), 143106.

[43] J. Philip, G. Gnanaprakash, G. Panneerselvam, M. P. Antony, T. Jayakumar, and B. Raj, Magnetic properties of $ZnFe_2O_4$ ferrite nanoparticles embedded in ZnO matrix, J. Appl. Phys. **102** (2007), 054305.

[44] A. M. Mudarra Navarro, C. E. Rodríguez Torres, V. Bilovol, A .F. Cabrera, L. A. Errico, and M. Weissmann, Study of the relation between oxygen vacancies and ferromagnetism in Fe-doped TiO_2nano-powders, Journal of Applied Physics **115** (2014), 223908.

[45] A. M. Mudarra Navarro, C. E. Rodríguez Torres, A. F. Cabrera, M. Weissmann, K. Nomura, and L. Errico, *Ab initio* study of the ferromagnetic response, local structure, and hyperfine properties of Fe-doped SnO_2, J. Phys. Chem. C **119** (2015), 5596.

[46] Ching Cheng, Long-range antiferromagnetic interactions in $ZnFe_2O_4$ and $CdFe_2O_4$: Density functional theory calculations, Phys. Rev. B **78** (2008), 132403.

[47] J. J. Melo Quintero, C.E. Rodríguez Torres, and L. A. Errico, *ab initio* calculation of structural, electronic and magnetic properties and hyperfine parameters at the Fe sites of pristine $ZnFe_2O_4$, J. Alloys and Comp.**741** (2018), 746.

[48] Jinhuan Yao, Yanwie Li, Xuanha Li, and Xiaodong Zhu, First-Principles Study of the Geometric and Electronic Structures of Zinc Ferrite with Vacancy Defect, Metallurgical and Materials Transactions A**47** (2016), 3753.

[49] J. Smit, H. P. J. Wijn, *Ferrites*, Philips Technical Library, 1959.

[50] J.A. Gomes, M.H. Sousa, F.A. Tourinho, J. Mestnik-Filho, R. Itri, J. Depeyrot, Rietveld structure refinement of the cation distribution in ferrite fine particles studied by X-ray powder diffraction, J. Magn. Magn.Mater.**289** (2005)184.

[51] U. Köning, E. F. Bertaut, Y. Gros, G. Chol, Models of the magnetic structure of zinc ferrite, Solid State Commun. **8** (1970) 759.

[52] B.J. Evans, S. S. Hafner, H. P. Weber, Electric field gradients at ^{57}Fe in $ZnFe_2O_4$and $CdFe_2O_4$, J. Chem. Phys. **55** (1971) 5282.

[53] A. Kremenovica, B. Antic, P. Vulic, J. Blanusa, A. Tomic, $ZnFe_2O_4$ antiferromagnetic structure redetermination, J. Magn. Magn. Mater. **426** (2017)264.

[54] P. Hohenberg and W. Kohn, Inhomogeneous Electron Gas, Phys. Rev. 136 (1964), B864.

[55] W. Kohn and L. J. Sham, Self-Consistent Equations Including Exchange and Correlation Effects, Phys. Rev. **140** (1965), A1133.

[56] S. Cottenier, Density Functional Theory and the Family of (L)APW-methods: aStep-by-Step Introduction, KU Leuven, Belgium, 2002. http://www.wien2k.at/reg_user/textbooks.

[57] Z. Wu and R. E. Cohen, More accurate generalized gradient approximation for solids, Phys. Rev. B **73**(**2006)**, 235116.

[58] V. I. Anisimov, I. V. Solovyev, M. A. Korotin, M. T. Czyzyk, G. A. Sawatzky, Density functional theory and NiO potoemission spectra, Phys. Rev. B **48** (1993), 16929.

[59] E. Sjöstedt, L. Nordström, D.J. Singh, An alternative way of linearizing theaugmented plane-wave method, Solid State Commun. **114** (2000) 15e20.

[60] G. K. H. Madsen, P. Blaha, K. Schwarz, E. Sjöstedt, L. Nordströom, Efficient linearization of the augmented plane-wave method, Phys. Rev. B **64** (2001),195134.

[61] P. Blaha, K. Schwarz, G. Madsen, D. Kvasnicka, J. Luitz, *WIEN2k, an Augmented Plane Wave Plus Local Orbitals Program for Calculating Crystal Properties*, Technical Universität Wien, Austria, 1999.

[62] G. Schatz, A. Weidinger, *Nuclear Condensed Matter Physics-Nuclear Methods and Applications*, Wiley, Chichester, 1996.

[63] P. Gütlich, E. Bill, A.X. Trautwein, *Mössbauer Spectroscopy and Transition Metal Chemistry*, Springer-Verlag, Berlin, Heidelberg, 2011.

[64] P. Novak, V. Chlan, Contact hyperfine field at Fe nuclei from density functional calculations, Phys. Rev. B **81** (2010), 174412.

[65] A. Manikandan, J. Judith Vijaya, M. Sundararajan, C. Meganathan, L. J. Kennedy, M. Bououdina, Optical and magnetic properties of Mg-doped$ZnFe_2O_4$ nanoparticles prepared by rapid microwave combustion method, Superlattices Microstruct. **64** (2013) 118.

[66] J. Yao, X. Li, Y. Li, and S. Le,Density Functional Theory Investigations on theStructure and Electronic Properties of Normal Spinel $ZnFe_2O_4$, Integr.Ferroelectr.**145** (2013), 17.

[67] S. Duhalde, M. F. Vignolo, C. Chiliotte, C. E. Rodríguez Torres, L. A. Errico, A. F. Cabrera, M. Rentería, H. Sánchez and M. Weissmann, Appearance of room-temperature ferromagnetism in Cu-doped $TiO_{2-\delta}$ films, Phys. Rev. B **72** (2005), 161313 (R).

[68] R. F. W. Bader, *Atoms in Molecules: A Quantum Theory*, Oxford University Press, New York, 1994.

[69] J. J. Melo Quintero, K. L. Salcedo Rodríguez, G. A. Pasquevich, P. Mendoza Zélis, S.J. Stewart, C.E. Rodríguez Torres, and L.A. Errico, Experimental and *ab initio* study of the hyperfine parameters of $ZnFe_2O_4$ with defects, Hyperfine Interact. **237** (2016), 63.

[70] M. Niyaifar, Effect of Preparation on Structure and Magnetic Properties of $ZnFe_2O_4$, Journal of Magnetics **19** (2014), 101.

[71] J. Kanamori, Superexchange interaction and symmetry properties of electron orbitals, J. Phys. Chem. Solids **10** (1959), 87.

[72] E. Lima Jr., E. De Biasi, M. Vasquez Mansilla, M. E. Saleta, F. Effenberg, L. M. Rossi, R. Cohen, H. R. Rechenberg, and R. D. Zysler, Surface effects in the magnetic properties of crystalline 3 nm ferrite nanoparticles chemically synthesized, J. Appl. Phys. **108** (2010), 103919.

[73] J. Nasr Isfahani and V. Sepelak, A Mössbauer effect study, as the main key to the investigation of anomalous magnetic properties of MnZn nanoferrite, Iranian Journal of Physics Research **12** (2012), 33.

Fe position	FM	AF1	AF2	AF3	AF4	AF5	FERRI1	FERRI2
0.5; 0.5; 0.5	+	+	+	-	-	+	+	-
0.5; 0.25; 0.25	+	+	+	+	-	+	+	+
0.0; 0.0; 0.5	+	+	+	+	+	+	+	+
0.0; 0.75; 0.25	+	+	+	-	-	-	+	+
0.0; 0.5; 0.0	+	+	-	-	+	-	+	+
0.0; 0.25; 0.75	+	+	-	+	+	+	-	+
0.5; 0.0; 0.0	+	+	-	-	-	-	-	+
0.5; 0.75; 0.75	+	+	-	-	-	-	-	+
0.75; 0.75; 0.5	+	-	-	+	+	+	-	+
0.25; 0.5; 0.25	+	-	-	+	+	+	-	+
0.25; 0.25; 0.5	+	-	-	-	-	-	-	+
0.75; 0.0; 0.25	+	-	-	+	+	-	-	+
0.25; 0.75; 0.0	+	-	+	-	-	+	+	+
0.75; 0.5; 0.75	+	-	+	+	+	-	+	+
0.75; 0.25; 0.0	+	-	+	+	+	+	+	+
0.25; 0.0; 0.75	+	-	+	-	-	-	+	+

Table 1: The different spin configurations studied in this work. + (-) indicates the relative spin orientations.

Magnetic configuration	E (meV/$u.f.$)
FM	0
AF1	-30
AF4	-39
AF3	-40
AF5	-41
FERRI3	-43
AF2	-44

Table 2: Energy (E) per unit formula ($u.f.$) of the different magnetic arrangement studied for the case of reduced ZFO (ZnFe$_2$O$_{4-\delta}$, δ=0.125). Energies are referred to the ferromagnetic case. A more negative value for E indicates a more stable arrangement.

Normal ZFO		Partially inverted ZFO		Inverted ZFO	
Zn^A-ONN	Fe^B-ONN	Fe^A-ONN	Zn^B-ONN	Fe^A-ONN	Zn^B-ONN
2.00 [4]	2.04 [6]	1.92 [2]	2.09 [2]	1.92 [2]	2.11 [2]
		1.94 [2]	2.11 [2]	1.93 [2]	2.13 [2]
			2.13		2.15
			2.18		2.18

Table 3: Relaxed bond-lengths (in Å) between Fe/Zn atoms and its first neighbor oxygen atoms for the normal, inverted and partially inverted ZFO. In square brackets we indicate the multiplicity.

Magnetic configuration	E (meV/$u.f.$)
FM	0
AF1	-67
AF4	-75
AF3	-77
AF5	-80
AF2	-80
FERRI4	-86

Table 4: Energy/$u.f.$ of the different magnetic arrangement studied for the case of partially inverted ZFO, $(Zn_{1-\alpha}Fe_{\alpha})[Zn_{\alpha}Fe_{2-\alpha}]O_4$. Energies are referred to the ferromagnetic case.

		Fe at site A		Fe at site B	
	T_m (K)	BHF (T)	IS (mm/s)	BHF (T)	IS (mm/s)
Experiment, Ref. 72	4.4	49.7_6	0.25_3	52.3_8	0.36_4
Experiment, Ref. 73	4.2	48.91_2	0.262_1	49.37_7	0.369_5
Ab initio, (α=0.125), this work	0	49.4	0.30	51_1 *	0.38

Table 5: Results obtained in Mössbauer Spectrocopy (MS) experiments performed at the indicated temperatures T_M in $(Zn_{1-\alpha}Fe_{\alpha})[Zn_{\alpha}Fe_{2-\alpha}]O_4$ nanoparticles and *ab initio* predictions the IS and the BHF. The theoretical results correspond to the lowest energy spin configuration (FERRI4). *: average value over the 15 Fe at sites B of the structure.

	T_m (K)	α	QS (mm/s)	IS (mm/s)
Experiment, Ref. 70	300	0.0375	0.38	0.32
	300	0.15	0.41	0.32
	300	0.16	0.44	0.32
Ab initio, this work	0	0.125	0.19 (site*A*) 0.33$_9$ (site*B*) *	0.30 (site*A*) 0.38 (site*B*)

Table 6: Results obtained in Mössbauer Spectrocopy (MS) experiments performed at room temperature (paramagnetic system) in $(Zn_{1-\alpha}Fe_\alpha)[Zn_\alpha Fe_{2-\alpha}]O_4$ nanoparticles and *ab initio* predictions for the *QS* and *IS*. The theoretical results correspond to the lowest energy spin configuration (FERRI4). *: average value over the 15 Fe at sites *B* of the structure.

Magnetic configuration	E (meV/*u.f.*)
FM	0
AF1	-32
AF4	-37
AF3	-46
AF5	-49
AF2	-54
FERRI5	-62

Table 7: Energy/*u.f.* of the different magnetic arrangement studied for the case of partially inverted and reduced ZFO, $(Zn_{1-\alpha}Fe_\alpha)[Zn_\alpha Fe_{2-\alpha}]O_{4-\delta}$. Energies are referred to the ferromagnetic case.
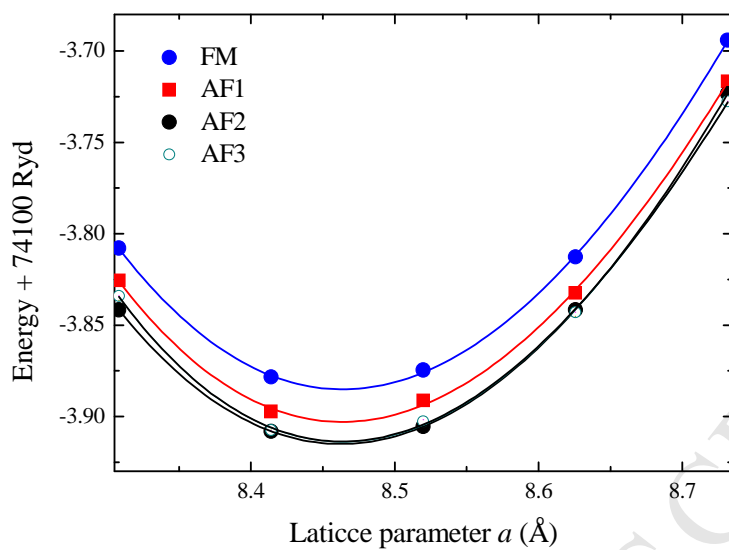
Figure 1: Calculated energy as a function of the lattice parameter a of reduced ZFO ($ZnFe_2O_{4-\delta}$) for different spin configurations. The minimum energy lattice parameter corresponds to 8.47 Å, a value that is nearly independently of the considered spin arrangement. For simplicity, the spin configurations AF4, AF5, FERRI1 and FERRI2 were not included in the figure (the energy differences between configurations AF3, AF4, and AF5 are includedin the size of the points).
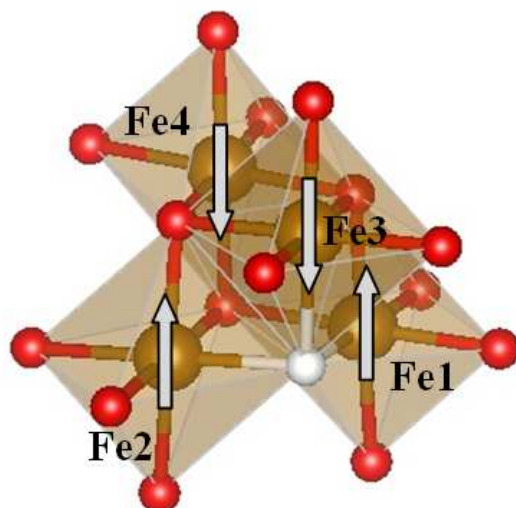
Figure 2: Portion of the un-relaxed spinel structure of $ZnFe_2O_{4-\delta}$. The Fe and O atoms are represented by gold and red spheres, respectively. The vacancy site is indicated by a white sphere. Arrows denotes the relative spin orientations of the Fe atoms. Fe1, Fe2 and Fe3 are the nearest neighbors atoms to the oxygen vacancy site and Fe4 is the second neighbor to the oxygen vacancy site.
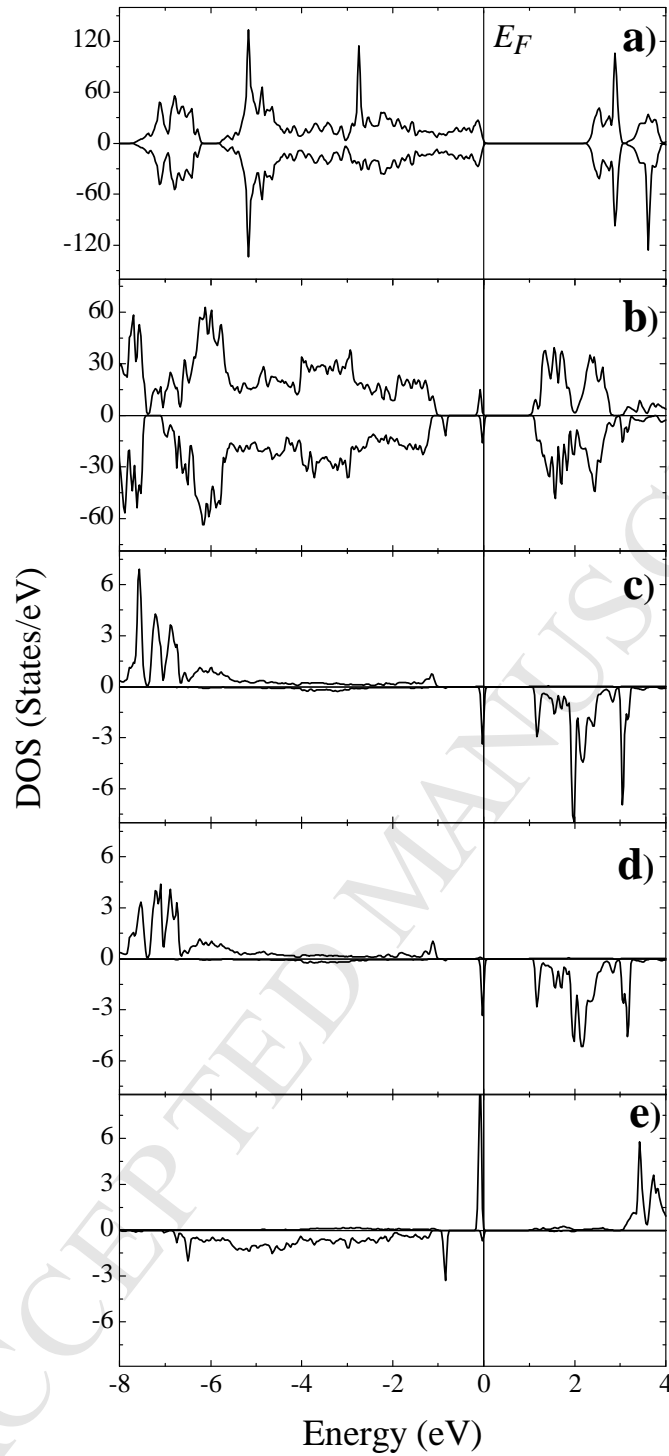
Figure 3: Calculated total density of states (DOS) of a) pristine ZFO; b) reduced ZFO ($ZnFe_2O_{4-\delta}$, δ=0.125) and partial DOS of Fe atoms nearest-neighborsto the vacancy sites c) Fe1-3d states; d) Fe2-3d states; e) Fe3-3$d$states. Energies are referred to the Fermi level (E_F), denoted by a vertical line. The results correspond to the AF2 spin configuration.
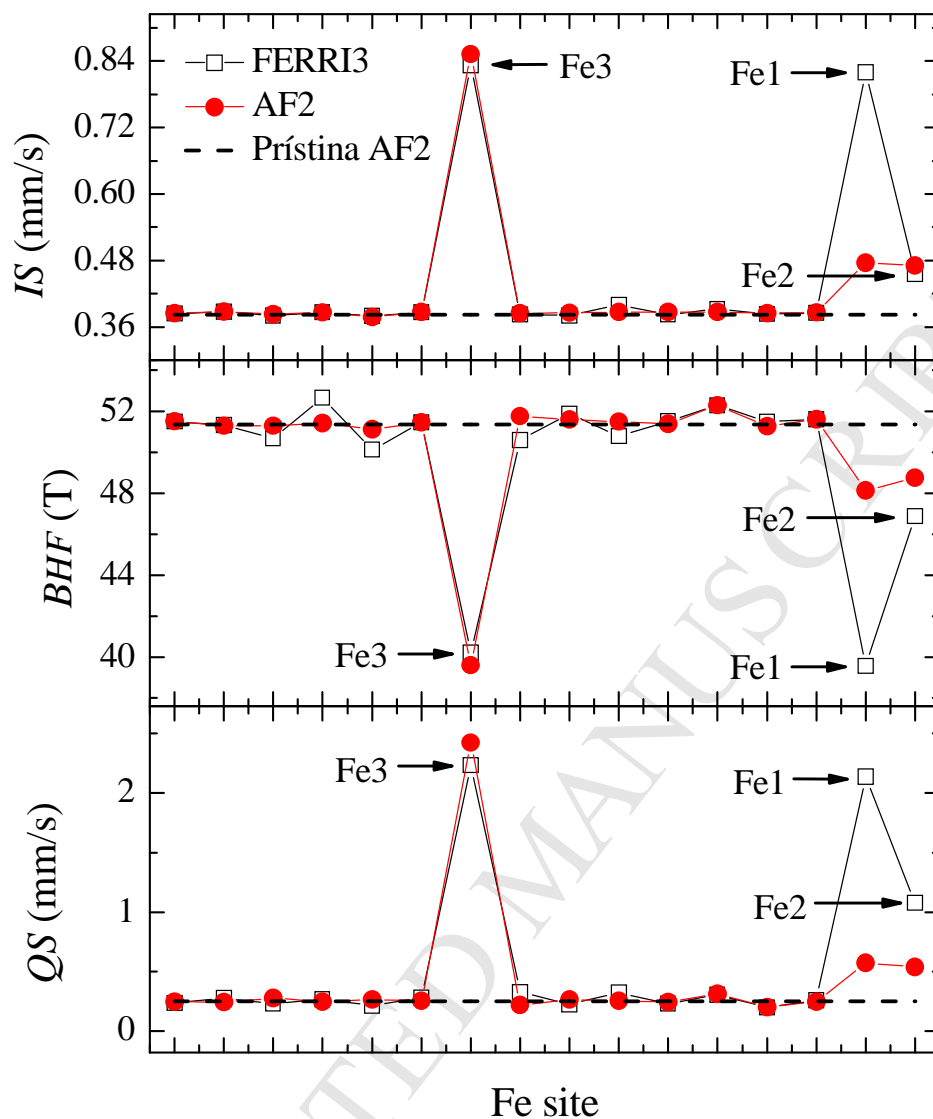
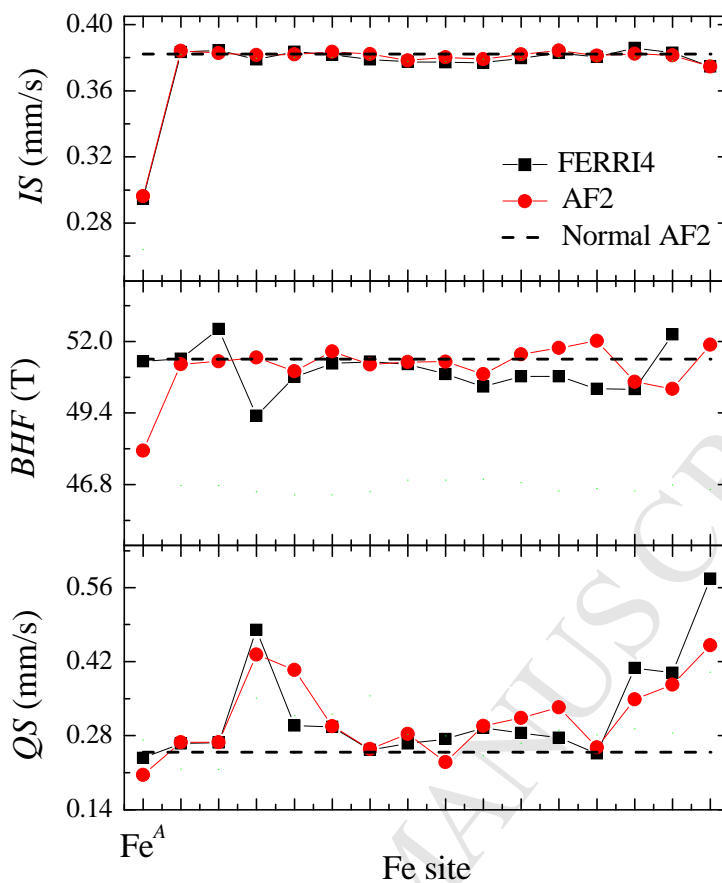Figure 4: Hyperfine parameters at the Fe sites of reduced ZFO, $ZnFe_2O_{4-\delta}$. The results correspond to the lowest energy spin configurations (AF2 and FERRI3). For the sake of comparison, the results for pristine ZFO (dashed lines) are also show.
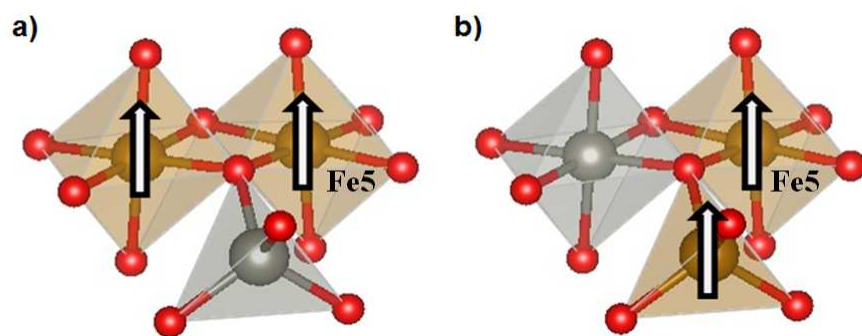
Figure 5: Schematic representation of inversion. Gold, grey, and red spheres represent Fe, Zn, and O atoms, respectively. a) Normal ZFO (two Fe located at sites *B*, and a Zn at site *A*). b) Inverted ZFO (a Fe and a Zn located at sites *B* and a Fe at site *A*). Arrows denotes the relative spin orientations in the AF2 configuration.
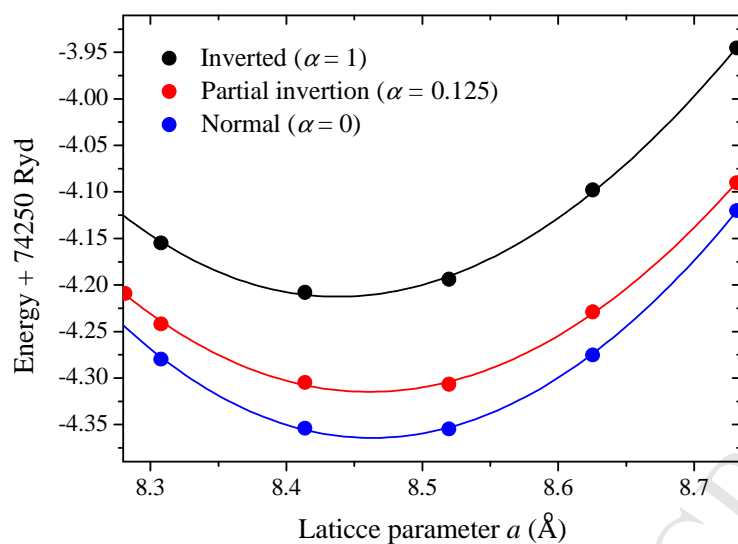
Figure 6: Total energy as a function of the lattice parameter a of normal, partially inverted ($\alpha = 0.125$) and inverted ($\alpha = 1$) $(Zn_{1-\alpha}Fe_{\alpha})[Zn_{\alpha}Fe_{2-\alpha}]O_4$. The E Vs. a curves correspond, in each case, to the lowest energy spin configurations.
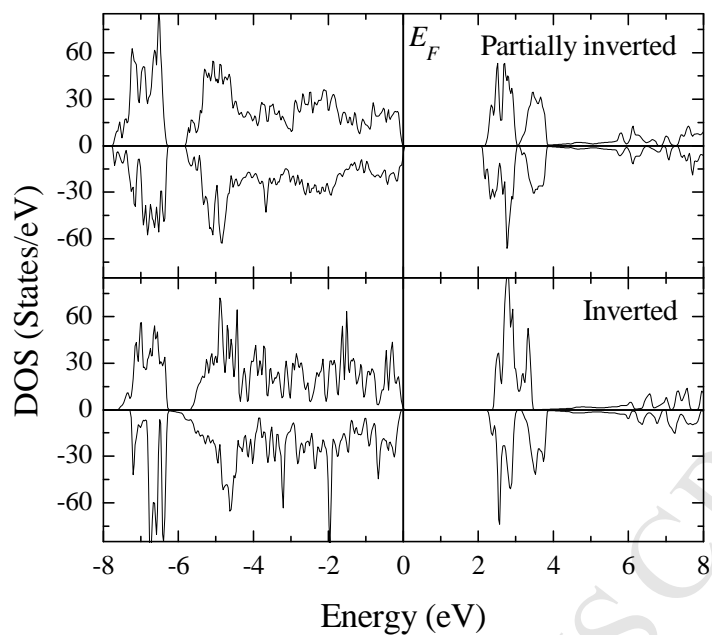
Figure 7: Calculated total density of states (DOS) of partially inverted (α =0.125) and inverted (α =1) $(Zn_{1-\alpha}Fe_{\alpha})[Zn_{\alpha}Fe_{2-\alpha}]O_4$. Energies are referred to the Fermi level (E_F), denoted by a vertical line. The results correspond to the AF2 configuration.

Figure 8: *ab initio* predictions for the hyperfine parameters at Fe sites of $(Zn_{1-\alpha}Fe_{\alpha})[Zn_{\alpha}Fe_{2-\alpha}]O_4$, α=0.125. Fe^A indicates the Fe atom in site *A*. For the sake of comparison, the results for normal ZFO (dashed horizontal lines) are also show. The results correspond to the lowest energy (FERRI4) and the AF2 configurations.
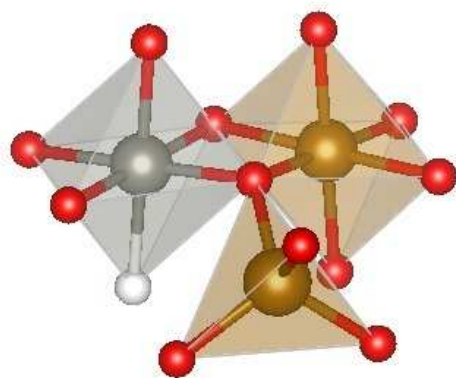
Figure 9: Portion of the ZFO cell with partial inversion (a Fe and a Zn located at sites *B*, and a Fe at site *A*) and an oxygen vacancy. Gold, grey, and red spheres represent Fe, Zn, and O atoms respectively. The vacancy site is indicated by a white sphere.
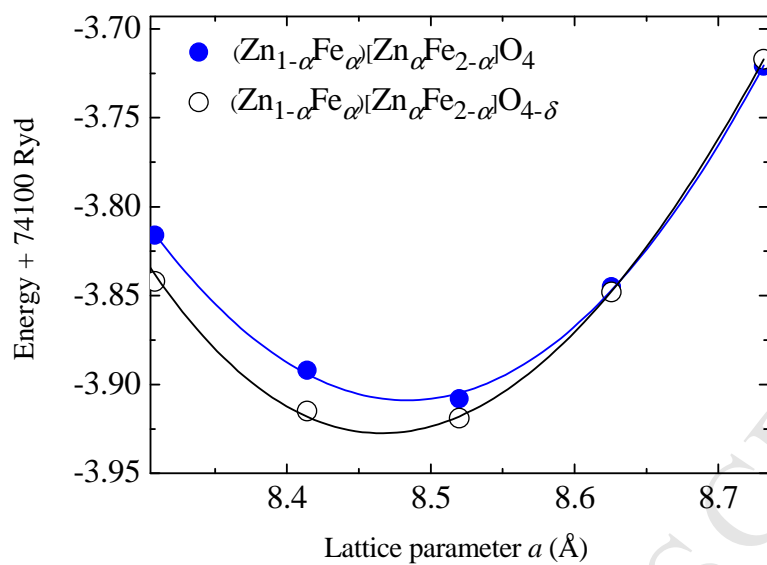
Figure 10: Energy as a function of a for reduced ZFO with normal structure ($ZnFe_2O_{4-\delta}$) and partially inverted structure, $(Zn_{1-\alpha}Fe_\alpha)[Zn_\alpha Fe_{2-\alpha}]O_{4-\delta}$.

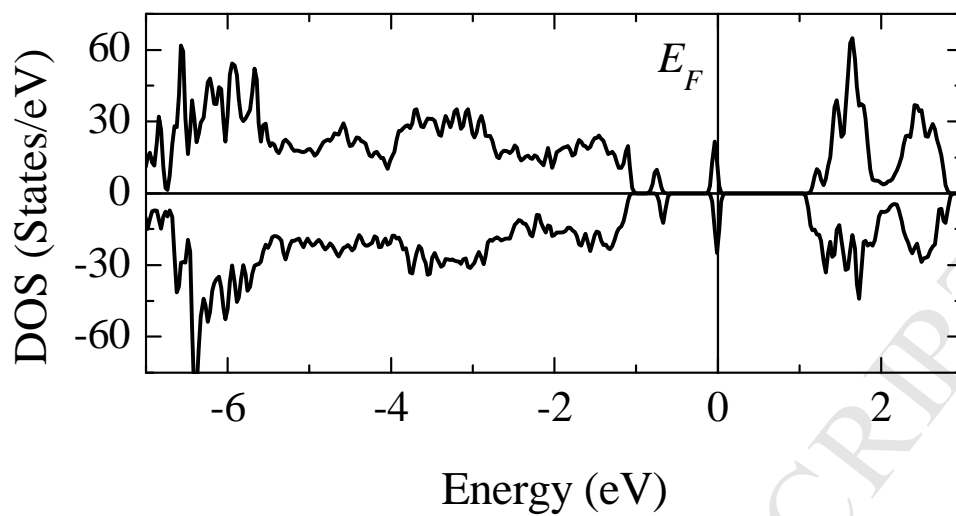Figure 11: DOS of partially inverted and reduced ZFO, $(Zn_{1-\alpha}Fe_\alpha)[Zn_\alpha Fe_{2-\alpha}]O_{4-\delta}$.

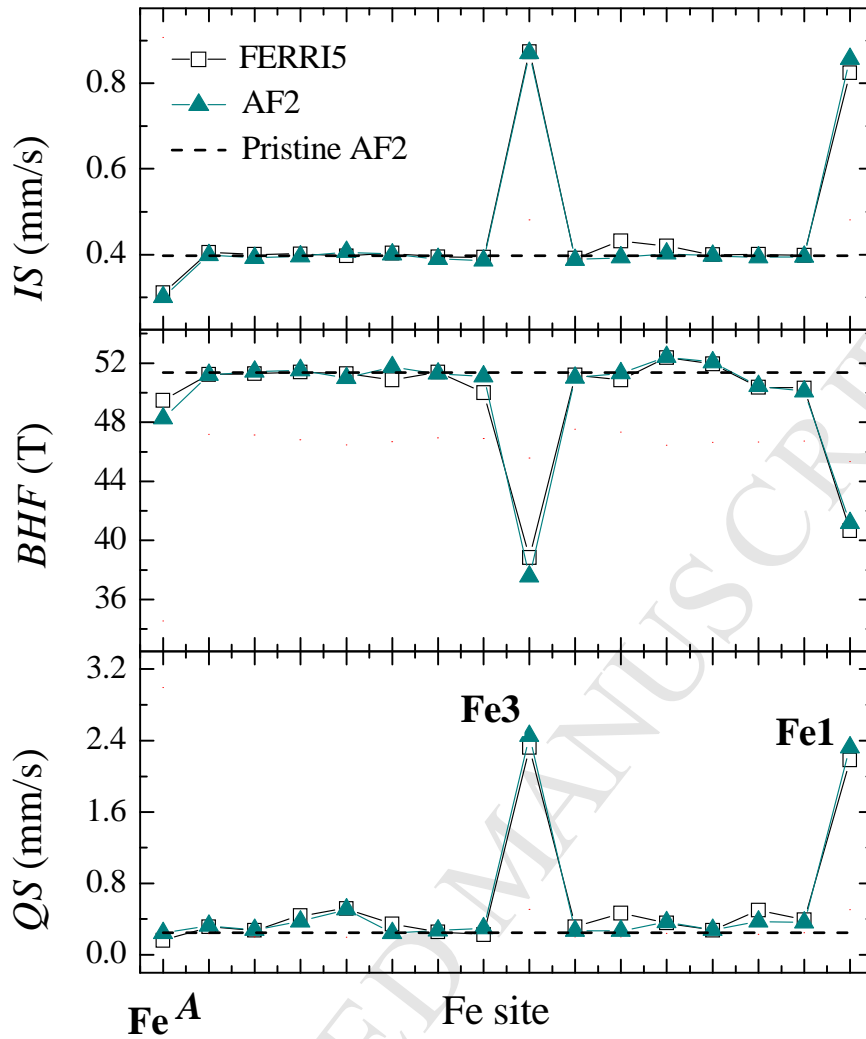Figure 12: *ab initio* predictions for the hyperfine parameters at the Fe sites of reduced and partially inverted $(Zn_{1-\alpha}Fe_{\alpha})[Zn_{\alpha}Fe_{2-\alpha}]O_{4-\delta}$ for the lowest energy (FERRI5) and the AF2 spin configurations. For the sake of comparison, the results for pristine ZFO are also show.

DFT study of structural, electronic and magnetic properties of defective $ZnFe_2O_4$.

Prediction of the hyperfine parameters at Fe sites of reduced and inverted $ZnFe_2O_4$.

Characterization of the electronic and magnetic structure at the Fe sites.

Defects favour a ferromagnetic coupling of Fe atoms.

Oxygen vacancies and antisites give rise to a ferrimagnetic ordering of $ZnFe_2O_4$.